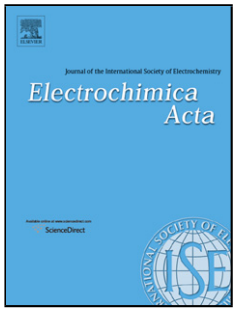

Title: Insight into CO Activation over Cu(100) under Electrochemical Conditions

Author: Tian Sheng Dong Wang Wen-Feng Lin P. Hu Shi-Gang Sun

PII: S0013-4686(16)30037-8
DOI: http://dx.doi.org/doi:10.1016/j.electacta.2016.01.037
Reference: EA 26419

To appear in: *Electrochimica Acta*

Received date: 13-7-2015
Revised date: 5-1-2016
Accepted date: 5-1-2016

Please cite this article as: Tian Sheng, Dong Wang, Wen-Feng Lin, P.Hu, Shi-Gang Sun, Insight into CO Activation over Cu(100) under Electrochemical Conditions, Electrochimica Acta http://dx.doi.org/10.1016/j.electacta.2016.01.037

Insight into CO Activation over Cu(100) under Electrochemical Conditions

Tian Sheng[a*], Dong Wang[b,c], Wen-Feng Lin[d], P. Hu,[b,c], Shi-Gang Sun[a*]

tsheng@xmu.edu.cn sgsun@xmu.edu.cn

[a]Collaborative Innovation Center of Chemistry for Energy Materials, State Key Laboratory of Physical Chemistry of Solid Surfaces, College of Chemistry and Chemical Engineering, Xiamen University, Xiamen, 361005, P. R. China.

[b]Key Laboratory for Advanced Materials, Centre for Computational Chemistry and Research Institute of Industrial Catalysis, East China University of Science and Technology, Shanghai, 200237, P. R. China.

[c]School of Chemistry and Chemical Engineering, Queen's University of Belfast, Belfast, BT9 5AG, U.K.

[d]Department of Chemical Engineering, Loughborough University, Loughborough, Leicestershire, LE11 3TU, UK.

[*]Corresponding authors

Highlights

(i) Adsorbed CO is negatively charged on Cu(100) and the aqueous solution leads to more negative charges on CO_{ads}.

(ii) For the formation of COH_{ads}, the reaction energy is endothermic by 0.34 eV and the free energy barrier is 0.38 eV, and the feasible route of proton transfer is illustrated.

(iii) A linear relationship is revealed between the C-O bond distance and the negative charge in CO.

(iv) The formation of CHO_{ads} is endothermic by 0.46 eV with the free energy barrier of 0.64 eV. Before the coupling, H adsorbs first with a reaction energy of -0.24 eV and the free energy barrier of 0.56 eV.

(v) The formation of COH_{ads} has been found to be more favorable than that of CHO_{ads} kinetically, but CHO_{ads} has been shown to be more stable thermodynamically.

Abstract

The reduction of CO_2 on copper electrodes has attracted great attentions in the last decades, since it provides a sustainable approach for energy restore. During the CO_2 reduction process, the electron transfer to CO_{ads} is experimentally suggested to be the crucial step. In this work, we examine two possible pathways in CO activation, i.e. to generate COH_{ads} and CHO_{ads}, respectively, by performing the state-of-the-art constrained *ab initio* molecular dynamics simulations on the charged Cu(100) electrode under aqueous conditions, which is close to the realistic electrochemical condition. The free energy profile in the formation of COH_{ads} via the coupled proton and electron transfer is plotted. Furthermore, by Bader charge analyses, a linear relationship between C-O bond distance and the negative charge in CO fragment is unveiled. The formation of CHO_{ads} is identified to be a surface catalytic reaction, which requires the adsorption of H atom on the surface first. By comparing these two pathways, we demonstrate that kinetically the formation of COH_{ads} is more favored than that of CHO_{ads}, while CHO_{ads} is thermodynamically more stable. This work reveals that CO activation via COH_{ads} intermediate is an important pathway in electrocatalysis, which could provide some insights into CO_2 electroreduction over Cu electrodes.

Keywords: CO_2; copper electrode; electroreduction; density functional theory; *ab initio* molecular dynamics.

1. Introduction

Electrocatalytic reduction of CO_2 into hydrocarbon fuels is a promising carbon cycle process for the sustainable energy storage, which was discovered by Hori et al.[1] In the last three decades, it has drawn great attentions thanks to the advantages of the electroreduction of CO_2 on copper electrodes with a high faradic efficiency occurring in aqueous electrolytes at ambient temperature.[1-5] To date, the copper electrode was found to be uniquely able to reduce CO_2 into hydrocarbons (methane and ethylene) in experiments.[6] Hori et al carried out the CO_2 electroreduction over a series of single crystal planes. Among them, Cu(100) performed a comparable activity to Cu(111), but the selectivity towards ethylene on Cu(100) is much higher.[7-9] To understand these observations, the reaction mechanisms have extensively been investigated using many methods.[10-15] The rate-determining step was suggested to be the electron transfer to the adsorbed CO, and the adsorbed COH was identified to be the crucial intermediate in the electroreduction of CO_2.[10-15] Recently, density functional theory (DFT) calculations were widely used for understanding the heterogeneous catalysis at atomic and molecular levels.[16-21] Norskov's group has developed a computational hydrogen electrode model to map out the free energy diagrams from CO_2 to CH_4 included about 40 elementary steps on Cu(111). By shifting the stability of intermediates in the diagrams via adjusting the electrode potential, this model explains successfully why such a negative potential (~-1 V vs SHE) was required in the electroreduction of CO_2.[17]

To capture the features of the electrical double layer where the reaction occurs in

electrocatalysis, some theoretical models were utilized using DFT calculations and molecular dynamics (MD) simulations.[22-32] In some studies, with the addition of extra electrons into the unit cell, the electrode potential could be controlled by the calculation of work function.[22-29] In other investigations, to avoid the introduction of artificial counter-charge, H atoms were introduced into the water layer which could separate into protons and electrons. Thus, one may vary the surface charge and the potential by changing the concentration of protons.[30, 31] Another significant challenge in modeling the electrical double layer is the aqueous solution, which is constantly fluctuating at the electrode under dynamic conditions.[25, 28, 32] As we all know that the presence of aqueous solution has a great impact on thermodynamics and kinetics of electrocatalytic reactions, and thus MD study is highly desired for describing the roles of solution in electrochemistry.

The coupling between proton and electron transfer ($H^+ + e^-$) is one of the key steps in electrochemistry, which plays significant roles in mutual conversions between chemical energy and electrical energy. For instance, with the separation of H atoms into protons and electrons, the oxidation of methanol or some other organic molecules to CO_2 could occur as the anodic reaction in fuel cell ($CH_3OH + H_2O \rightarrow CO_2 + 6H^+ + 6e^-$), which is a promising energy solution in place of fossil fuels.[33] On the other hand, with the combination of protons and electrons at the interface, hydrogen evolution ($2H^+ + 2e^- \rightarrow H_2$) and CO_2 reduction ($CO_2 + 8H^+ + 8\ e^- \rightarrow CH_4 + 2H_2O$) could effectively convert electrical energy into chemical energy. Therefore, the understanding of the coupling between proton and electron transfer at atomic level is

of great importance in electrocatalysis. However, to the best of our knowledge, the investigation of this process using MD calculations is still missing in electrocatalysis. Most of the previous theoretical works were performed by using the vacuum model or static water structure since the MD simulation is extraordinary time consuming.[18-20, 22, 23]

In comparison with Cu(111),[17, 19, 20] Cu(100) was relatively less reported in the current theoretical work.[21] Based on experimental work, Schouten et al suggested that the behaviors of Cu polycrystalline and Cu(100) are very much alike in terms of the remarkable CO_2 reduction selectivity towards ethylene, and thus inferring that the dominating facet of Cu polycrystalline is actually Cu(100) instead of Cu(111).[34] Using *operando* electrochemical scanning tunneling microscopy (EC-STM), Kim et al also observed the reconstruction of Cu(111) to Cu(100) under the CO_2 electroreduction condition but no further transformation from Cu(100).[35] Therefore, Cu(100) is probably more stable and acts as the real reactive surface in CO_2 electroreduction.

Herein, we focus on the CO activation over Cu(100) surface in this work. By performing the state-of-the-art constrained *ab initio* MD simulations, we investigated two possible pathways in CO activation to produce CHO_{ads} and COH_{ads}, respectively, at a charged water/Cu(100) interface for modelling the realistic electrochemical condition. We found that the formation of COH_{ads} via a coupling mechanism between proton and electron transfer would kinetically be more favored than that of CHO_{ads} via a surface catalytic mechanism, although CHO_{ads} is proved to be more stable than

COH_{ads}. The paper is organised as follows. In section 2, computational details are presented. In section 3, analyses of charge distribution at the interface, electrode potentials, reaction free energies, structure evolution and electron transfer are illustrated. In section 4, the two CO activation pathways, the constant potential issue, the computational hydrogen electrode method and H_{ads} coverage effect are discussed. Finally, in section 5 our results are summarized.

2. Computational details

All the electronic structure calculations were carried out using the Vienna Ab-initio Simulation Package (VASP) with Perdew-Burke-Ernzerh (PBE) functional of exchange-correlation. The projector-augmented-wave (PAW) pseudopotentials were utilized to describe the core electron interaction.[36-43] It is worth mentioning that the intrinsic delocalization error of PBE, higher than B3LYP in describing the proton and electron transfer, could introduces some errors in the calculated results.[44] The open Cu(100) surface was modeled by *p*(3x3) unit cell with four layers. The bottom two layers were fixed and the top two layers were fully relaxed during *ab initio* MD simulation. The cut-off energy was set as 400 eV and a $3\times3\times1$ Monkhorst-Pack k-point sampling was used for calculating the free energy. The MD simulations were performed within the canonical (NVT) ensemble by Nosé-Hoover thermostat method at a constant temperature of 300 K (SMASS>=0). In order to simulate the electrical double layer, a charged aqueous interface model was used, which contains 20 water molecules and one H atom inside the water layer. The

density of water layer was kept constant at 1 g cm^{-3} during the MD simulation. Considering that the water layer was relatively thin (~12 Å) and the bottom of Cu slab would affect the water structure, a vacuum layer of 7 Å was therefore added above the water layer to avoid the interaction between water molecules and the bottom of Cu slab. The model used in this work is presented in **Figure 1**. In the calculation of work function (Φ), a long time *ab initio* molecular simulation (20 ps) was performed. Because the work function of the system was found to be quite sensitive to water orientations,[27, 30] we calculated the work function of 20 structures from the last 5 ps MD simulation, and further averaged them as the representative value for the system. The calculated work functions of these 20 samples are listed in **Table S1**. The electrode potential (U) was obtained by referring the work function of the system to the experimental work function of standard hydrogen electrode (SHE) according to the following equation, $U = \Phi/e - 4.44$.[22, 23]

The constrained *ab initio* MD method was well established on the basis of thermodynamic integration by Sprik and others,[46-48] and here we employed it to calculate the free energy of reactions at the aqueous interface. The dipole correction was not included in the MD simulation. For each state we performed *ab initio* MD simulation for 6 ps (1 fs per step, 6000 steps) at a constant room temperature (T = 300 K) until the interatomic forces were converged. The difference of interatomic force was found to be negligible between using a step length of 1 fs per step and 0.5 fs per step. We also found that the interatomic force starts usually to converge after a MD duration of at least 3 ps. To be accurate, we only selected the samples from the last 1

ps (1000 samples) of each MD simulation to do the average of the interatomic force, which was much longer than the oscillation period (~50 fs). Similarly, the C-O bond lengths were also averaged from the six samples within the last 1 ps MD simulation. All of the detailed data are listed in **Table S2**.

3. Results

3.1 Charged aqueous interface model

When an extra H atom is manually added into the aqueous solution consisting of 20 water molecules, H atom spontaneously separates into a solvated proton (H^+) in solution and an electron ending up at the slab. Bader charge analysis shows that the solvated proton (H^+) has positive charges of 0.55 e, which is close to the charge of OH^- anion in sodium hydroxide solution (-0.62 e) quantitatively.[32] The solvated H^+ prefers to bind to water molecules and three complex structures are observed during the MD simulation. The simplest structure is H_3O^+ in which H^+ binds to only one single water molecular. H^+ can also be shared by two or three water molecules in forms of $H_5O_2^+$ or $H_7O_3^+$, respectively. Compared with the static electrical double layer model in which H^+ is froze in the first water layer without dynamics, our model describes well the dynamic nature of H^+ in aqueous solution.[16, 18] In addition, since the introduction of electrons, each different proton concentration corresponds to a certain electrode potential versus the standard hydrogen electrode (SHE), thus indicating that varying the proton concentration can adjust the electrode potential.[30] The electrostatic potential is plotted in **Figure 2** and the standard deviations are listed

in **Table S1**. One can see that the work function is 3.81±1.23 eV in neutral system and thus, the corresponding electrode potential (potential of zero charge) is -0.63 (vs SHE), which is close to the experimental value of -0.54 V (vs SHE).[50] In the charged interface model including H^+, the work function is decreased to be 2.40±0.29 eV and the corresponding electrode potential is -2.04 V (vs SHE), which is lower than the onset potential of -1.39 V (vs SHE) in CO_2 electroreduction on Cu(100) in ref [8].

Aiming to understand the CO adsorption at the electrode, we investigated the electron transfer between Cu(100) and CO_{ads} using three different models: (i) CO adsorption at Cu(100) without water; (ii) CO adsorption at the water/Cu(100) interface (20 water molecules); and (iii) CO adsorption at the charged water/Cu(100) interface (20 water molecules with H^+). Bader charge results are listed in **Table 1.** We found that CO_{ads} is negatively charged by spontaneously abstracting electron from Cu slab. Without water molecules, the quantity of negative charge of CO_{ads} is -0.44 e. In neutral aqueous solution, CO_{ads} is more negatively charged (-0.65 e vs -0.44 e), indicating that water can effectively facilitate the electron transfer from Cu to CO_{ads}. This result can be understood by the stronger interaction between CO_{ads} and Cu(100) as a consequence of hydrogen bonding. In the third model, when adding a H atom into the aqueous solution, the separated electron (-0.59 e) would enter into the CO/Cu(100) slab. However, only -0.09 e are captured by CO_{ads} while -0.46 e are delocalized in the Cu slab. Nevertheless, -0.09 e lengthens the C-O bond from 1.218 Å to 1.273 Å, implying that negative potential could activate CO_{ads}.[15]

3.2 Formation of COH

As for the formation of COH_{ads}, there are two possible pathways: (i) $CO_{ads} + H^+ + e^- \rightarrow COH_{ads}$, in which H^+ attacks CO_{ads} directly from the solution; and (ii) $CO_{ads} + H_{ads} \rightarrow COH_{ads}$, in which H^+ firstly adsorbs on Cu(100) yielding H_{ads}, and then transfers to CO_{ads} via a surface catalytic process. Aiming to identify the energetically favorable pathway, we examined systematically the both pathways. From the MD simulations, we found that pathway ii changes spontaneously to path i, since the constrained H atom is solvated in aqueous solution into H^+ very quickly when the distance between the H and the O is smaller than ~1.4 Å. It suggests that the transition state in path ii is extremely unstable, and thus it is the H^+ from the solution instead of H_{ads} on the surface that is more likely to attack the O-end of CO. Without water molecules, the reaction barrier in path ii is as high as 2.31 eV, which also explains the spontaneous change from path ii to path i in the MD simulation. The transition state in path ii without water molecules is shown in **Figure S1**. The favored mechanism of the COH_{ads} formation is described as reaction 1 and the free energy profile is plotted in **Figure 3**.

$$CO_{ads} + H^+ + e^- \rightarrow COH_{ads} \qquad (1)$$

3.2.1 Proton transfer

At the initial state, the distance between H^+ and O-end of CO_{ads} was set to be 1.8 Å. H^+ prefers to freely diffuse in aqueous solution in the form of H_3O^+ or $H_5O_2^+$ or $H_7O_3^+$ rather than staying near CO_{ads} which is thought to be the reactive centre. As the

distance shortens to 1.5 Å, H^+ is still free in aqueous solution as shown in **Figure 4a** and **4b**. When H^+ approaches the O-end of CO_{ads} at the distance of 1.4 Å, $H_5O_2^+$ species is found close to CO_{ads} with the structure of $[CO_{ads}\ldots H_5O_2^+{}_{aq}]$ as illustrated in **Figure 4c**, indicating that from this distance on H^+ is ready for transferring. Then, at the distance of 1.3 Å, $[CO_{ads}\ldots H_5O_2^+{}_{aq}]$ breaks into $[CO_{ads}\ldots H_3O^+{}_{aq}]$ with the release of one water molecule into solution, and H^+ is now co-stabilized by H_2O and CO_{ads}, as shown in **Figure 4d**. As the distance between H^+ and O-end of CO_{ads} are close to around 1.2 - 1.1 Å, the structure reaches the transition state, where the original O-H bond in H_3O^+ breaks and the new O-H bond in COH_{ads} forms (**Figure 4e** and **4f**), and the free energy reaches the highest position of 0.38 eV at the transition state in the case of ~1.14 Å. Then, the distance between H^+ and the binding water elongates gradually from 1.12 Å to 1.36 Å. It should be noted that because of the limitation of constrained MD approach, the well-defined transition state may not exactly be located along the reaction path. Afterwards, as **Figure 4g** shows, $[CO_{ads}\ldots H_3O^+{}_{aq}]$ is completely broken into COH_{ads}, and the distance between H^+ and the nearest water molecular is 1.73 Å. This step is endothermic by 0.34 eV and the free energy barrier is 0.38 eV.

To demonstrate the coupled proton and electron transfer, we analysed the charge distribution in the new formed COH_{ads}. COH_{ads} is negatively charged by -0.52 e, in which the CO fragment possesses -1.19 e and the H fragment holds 0.67 e. It indicates that the H fragment keeps the characteristics of proton by the polarization of $CO^{\delta-}$-$H^{\delta+}$ bond. In comparison with the initial CO_{ads} (-0.74 e), an extra -0.45 e is abstracted

from the Cu slab. According to the change of H^+ structures, the proton transfer route could be written as

$$CO_{ads} + H_5O_2^+{}_{aq} \rightarrow [CO_{ads}\ldots H_5O_2^+{}_{aq}] \quad (2)$$

$$[CO_{ads}\ldots H_5O_2^+{}_{aq}] \rightarrow [CO_{ads}\ldots H_3O^+{}_{aq}] + H_2O_{aq} \quad (3)$$

$$[CO_{ads}\ldots H_3O^+{}_{aq}] + e^- \rightarrow COH_{ads} + H_2O_{aq} \quad (4)$$

The rate-determining step in CO_2 electroreduction over the Cu electrode was experimentally suggested to be the electron transfer to CO_{ads}.[10-15] Our calculated results suggest that the driving force for the electron transfer from Cu(100) to CO_{ads} is the formation of the new O-H chemical bond between H^+ and O-end of CO_{ads}. With the assistance of proton transfer, the electron could be transferred to COH_{ads}.

3.2.2 Electron transfer

Our calculations show that in the formation to COH_{ads}, the electron is possessed by CO_{ads} on which a proton binds. To unveil the microscopic view of electron transfer, we quantified the negative charge in the CO fragment with approaching H^+. The results are presented in **Figure 5a** in which the electron transfer occurs rapidly near the transition state. From the initial distance of 1.8 Å to 1.2 Å, the negative charge in CO fragment increases slightly from -0.74 e to -0.83 e while the free energy rises as large as 0.35 eV. However, near the transition state at around 1.2 - 1.1 Å, the CO fragment is considerably more negatively charged from -0.84 e to -1.16 e, but the free energy hardly changes. Finally, the negative charges in CO fragment are -1.19 e. In order to provide more understandings on the electron transfer near the transition state

(~1.14 Å), we computed additionally four sets of different samples at the distances between H^+ and O atom of 1.18 Å, 1.16 Å, 1.14 Å and 1.12 Å, respectively. All the structures were obtained by running 6 ps *ab initio* MD simulations.

3.2.3 C-O bond length

In section 3.1, we showed that as small as -0.12 e negative charges on CO_{ads} can lengthen the C-O bond from 1.218 Å to 1.273 Å, implying that the negative charges can noticeably affect the C-O bond distance. Thus, we quantified systematically the C-O bond distance as H^+ approaches gradually the O-end of CO_{ads} during the formation of COH_{ads}. **Figure 5b** shows that the trend in the C-O bond distance is in good agreement with that in the electron transfer as presented in **Figure 5a**. Near the transition state, the C-O bond distance elongates dramatically from 1.264 Å to 1.359 Å accompanied with the increase of negative charges from -0.84 e to -1.16 e. It is worth mentioning that our results are statistically obtained from *ab initio* MD simulations at room temperature, and thus different numbers of samples could result in inevitable fluctuations of the data if the sample number were not completed. In general, we believe that the standard deviation listed in **Table S2** is competent in appropriately reflecting the trend. To further clarify the similar trend observed in **Figure 5a** and **5b**, we analyzed CO fragments under different conditions, i.e. CO and COH adsorption at Cu(100) without water, CO and COH adsorption at the water/Cu(100) interface, CO adsorption at the charged water/Cu(100) interface, and CO molecule in vacuum as a reference. **Figure 6** shows that the negative charges in

CO could linearly affects the C-O bond distance.

We should mention that the variation of electric field would affect C-O bond length due to the Stark effect in the formation of COH_{ads}.[50] Thus, we investigated the C-O bond length and its negative charges under an external electric field of ±0.52 V/Å. The results listed in **Table 4** were calculated without water, which are similar to the data reported in ref [50]. Assuming that the voltage drops over an electrical double layer with ~3 Å thickness,[45, 51] the corresponding electrode potential under ±0.52 V/Å would be ~ ±1.56 V (vs SHE). From our results, the electric field increases only the C-O bond length by 0.006 Å under 0.52 V/Å and decreases by -0.006 Å under -0.52 V/Å, which is smaller than the bond distance change of ~0.09 Å (from 1.273 Å to 1.361 Å) from CO_{ads} to COH_{ads}. Additionally, the poor electron transfer (i.e. -0.440 e under -0.52 V/Å, -0.443 e under 0.52 V/Å) also agrees well with the linear relationship in **Figure 6**. Therefore, we can confirm that the changes in the C-O bond length is mainly caused by the electron transfer to CO_{ads} instead of the electric field effect.

3.3 Formation of CHO

Regarding the formation of CHO_{ads}, there are also two possible pathways: (i) $CO_{ads} + H^+ + e^- \rightarrow CHO_{ads}$; and (ii) $CO_{ads} + H_{ads} \rightarrow CHO_{ads}$. It is different with the formation of COH_{ads} in which H^+ transfers directly to CO_{ads}, here path i was found to be unfavored for the formation of CHO_{ads}. During the MD simulation for path i, the constrained H^+ adsorbs spontaneously on the surface in a few fs, indicating that H_{ads}

prefers to associate with the C-end of CO_{ads} instead of H^+ in the solution. Therefore, the formation of CHO_{ads} can be divided into two steps:

$$H^+ + e^- \rightarrow H_{ads} \quad (5)$$

$$CO_{ads} + H_{ads} \rightarrow CHO_{ads} \quad (6)$$

The free energy profile for reactions 5 and 6 are displayed in **Figure 7**. H adsorption process was calculated to be exothermic by -0.24 eV with the free energy barrier of 0.56 eV, indicating that H_{ads} is more stable than solvated H^+ under the electrode potential of -2.04 V (vs SHE). The structures of H^+ adsorption from aqueous solution onto the Cu surface are presented from **Figure 8a** to **8e**. Initially, H^+ is solvated in aqueous solution in the form of $H_5O_2^+$, as shown in **Figure 8a** and **8b**. At the transition state with the distance of ~1.45 Å between H^+ and the binding O atom in water, H adsorbs at bridge site on Cu(100) (**Figure 8c** and **8d**). Afterwards, the O-H bond breaks, resulting in a H_{ads} adsorbed at hollow site (**Figure 8e**). The hydrogenation of CO_{ads} to CHO_{ads} is endothermic by 0.46 eV with the barrier of 0.64 eV. **Figure 8f** to **8j** present the structures in the order of gradually shortening the bond distance of C-H in the pathway. One can see that in **Figure 8f-h** both the H_{ads} and CO_{ads} move first from a hollow site to a bridge site and then the C-H bond association occurs at the distance of ~1.4 Å. After that, the O-end of CHO_{ads} adsorbs on the Cu(100) surface instead of dangling in water, which is the most stable configuration of CHO_{ads} (**Figure 8j**). Without water molecules, the formation of CHO_{ads} is endothermic by 0.72 eV with the reaction barrier of 0.92 eV. The transition and final states are stabilized by the aqueous solution of -0.26 eV and -0.28 eV respectively,

indicating that water could facilitate the CHO_{ads} formation. The transition state without water molecules is shown in **Figure S1**. Compared with the data obtained on Cu(111) where the reaction energy is 0.71 eV with a high barrier of 0.99 eV, Cu(100) is more active for the CHO_{ads} formation.[20]

4. Discussions

4.1 COH or CHO

As presented above, we have identified two feasible pathways for the formation of COH_{ads} and CHO_{ads} in CO activation on Cu(100), respectively. The free energy profiles of the favored pathways are shown in **Figure 9**. With respect to the initial state consisting of CO_{ads} and $H^+ + e^-$, the formation of COH_{ads} is endothermic by 0.34 eV which is higher than that of CHO_{ads} (0.22 eV), implying that CHO_{ads} is relatively more stable on the surface. However, kinetically the barrier in the formation of CHO_{ads} is 0.64 eV (reaction 6) which is higher than that of 0.38 eV (reaction 1) in the formation of COH_{ads}. Therefore, the formation of COH_{ads} is expected to be kinetically more favored. In comparison with previous work in which all the hydrogenation steps follow the Langmuir-Hinshelwood mechanism, i.e. the coupling of intermediate and surface H_{ads}[9, 20], in this work we revealed that the formation of COH_{ads} follows actually the coupled proton and electron transfer, which is regarded as a feature reaction in electrocatalysis. In addition, we use a dynamic water/metal interface model with many explicit water molecules, which is more accurate in describing the water effect than the vacuum/metal interface model with several static water

molecules.[19, 20, 52] However, for the favored pathway of the formation of COH_{ads} and that of CHO_{ads} formation, the current data cannot confirm whether it is one of the two contributes the most to the whole catalytic process in reality, or they are both reactive. It depends strongly on the subsequent reactions of the two intermediates and further investigates on the reactions are underway.

4.2 Constant potential effect

It is worth pointing out that in a real electrochemical system, the electrode potential is kept constant during the coupled proton and electron transfer. However, considering that the size of our model in this simulation is relatively small due to the computational limitation, the electrode potential would change significantly in the coupled proton and electron transfer (e.g. reaction 1). This crucial issue is still a huge challenge within DFT framework. To date, the accurate calculation of an electrocatalytic reaction involving the coupled proton and electron transfer is rather difficult since many factors (e.g. constant potential, pH and ion concentrations) are neglected in such a small unit cell. Some errors are inevitable in the current state of DFT, and the description of the electrocatalytic reactions is just an approximation. Nevertheless, the comparison between the two pathways in CO activation could help us to generally understand the realistic reaction mechanism at the atomic scale.

As displayed in **Figure 2**, the disappearance of H^+ results in an increase in the electrode potential from -2.04 V (vs SHE) to -0.63 V (vs SHE), thus introducing errors in the reaction energy and the activation barrier in reaction 1 and 5 involving

the coupled proton and electron transfer. Some possible errors are worth being discussed here. We note that, despite of the inconstant potential, it has hardly any noticeable influence on the understanding of the two competitive pathways in CO activation due to the following reasons. Liu's group reported that for the surface reaction which follows the Langmuir-Hinshelwood mechanism, e.g. reaction 6, it is usually insensitive to the electrode potential; however, for the reaction with the proton and electron transfer, which follows the Eley-Rideal mechanism, e.g. reaction 1, 5, it could be facilitated by negative electrode potential.[26, 53] By using computational hydrogen electrode model, it also suggests that a more negative electrode potential could make reaction 1 (COH_{ads}) and reaction 5 (H_{ads}) more exothermic, which will be discussed in the following section.[17] The realistic free energy profile at a constant potential is thus inferred as follows. At a constant potential of -2.04 V (vs SHE), the position of COH_{ads} and H_{ads} in the free energy diagram would shift down equally due to the involvement of one electron transfer. In contrast, since the formation of CHO_{ads} is a typical surface reaction which is rarely affected by the potential, the position of CHO_{ads} with respect to CO_{ads} + H_{ads} keeps fixed. Consequently, the relative position of COH_{ads} and CHO_{ads} in the free energy diagram is unchanged. More importantly, at a constant potential the formation of COH_{ads} is kinetically accelerated and thus, the barrier is actually lower than 0.38 eV while the barrier in the formation of CHO_{ads} is still 0.64 eV.[26, 53] Therefore, with all these analyses considered, the formation of COH_{ads} would kinetically be better than that of CHO_{ads}.

4.3 Computational hydrogen electrode model

Additionally, we calculated the formation of COH_{ads} and CHO_{ads} from the state of CO_{ads} and $H^+ + e^-$ using computational hydrogen electrode method in vacuum as a reference to avoid the varied potential in the proton transfer process.[17] The free energy profile is presented in **Figure 10**. It can be seen that, under the standard hydrogen electrode condition, the formation energies are 1.11 eV for COH_{ads} and 0.73 eV for CHO_{ads}, respectively. Under the external electrode potential of -2.04 V (vs SHE), the formations of COH_{ads} and CHO_{ads} would energetically be much favored with exothermic reaction energies of -0.94 eV and -1.31 eV, respectively. In the computational hydrogen electrode approach, the free energy of $H^+ + e^-$ equals to that of 1/2 H_2 under the standard hydrogen electrode condition. Consequently, a correction energy of -2.04 eV (eU) can directly be used to shift the relative energy of intermediates.[16]

However, in the investigation of coupled proton and electron transfer process in our model, the explicit coupled state of $H^+ + e^-$ was introduced at the water/Cu(100) interface. Thus, the combination of these two models can provide better understandings on the electrocatalytic reactions both thermodynamically and kinetically.[18] The different states of $H^+ + e^-$ in these two models would lead to different positions of initial states ($CO_{ads} + H^+ + e^-$) in the free energy diagram. In addition to this, the relative positions of COH_{ads} and CHO_{ads} are similar in both models as shown in **Figure 9** and **10**. Without water, CHO_{ads} is also more stable than COH_{ads} by 0.38 eV (0.12 eV in the presence of aqueous solution), indicating that the

aqueous solution stabilizes COH_{ads} more than CHO_{ads}. Therefore, the calculations using computational hydrogen electrode model can also provide evidence that CHO_{ads} is more stable than COH_{ads}, which supports our results in section 4.2.

4.4 H coverage effect

We note that H_{ads} is energetically more stable than solvated H^+ from **Figure 7** and thus the H_{ads} coverage effect on CO activation should be considered. We calculated systematically the reaction energy without water with an increase of H_{ads} coverage from 0 ML to 0.89 ML, and the results are plotted in **Figure 11a** and **Table S3**. One can see that the free energies for the formation of COH_{ads} and CHO_{ads} are not remarkably affected when the H_{ads} coverage is lower than 0.55 ML. Once the H_{ads} coverage is higher than 0.55 ML, the formation of COH_{ads} tends to be more difficult but the formation of CHO_{ads} is facilitated. However, a very high H_{ads} coverage was found to be unstable since the surface H_{ads} tends to couple with each other, generating H_2. Accordingly, the free energy of the reaction, $H_{ads} \rightarrow 1/2\ H_2$, is plotted against the H_{ads} coverage in **Figure 11b**. It can clearly be seen that, under high coverages of H_{ads}, the stability of $1/2\ H_2$ is much higher than that of H_{ads}. Therefore, we suggest that the H_{ads} coverage on Cu(100) is expected not to be high and thus its influence should be negligible.

5. Conclusions

In this work, the CO activation via two pathways to produce COH_{ads} or CHO_{ads}

on Cu(100) have been investigated at a charged aqueous interface. The mechanisms in the formations of COH_{ads} ($CO_{ads} + H^+ + e^- \rightarrow COH_{ads}$) and CHO_{ads} ($CO_{ads} + H_{ads} \rightarrow CHO_{ads}$) have been identified by computing the free energy barriers and the reaction energies using constrained *ab initio* molecular dynamics simulations. The main conclusions in this work are summarized below:

(i) Adsorbed CO is negatively charged on Cu(100) and the aqueous solution leads to more negative charges on CO_{ads}. At the charged aqueous interface, CO_{ads} possesses more electrons.

(ii) For the formation of COH_{ads}, the reaction energy is endothermic by 0.34 eV and the free energy barrier is 0.38 eV, indicating that the rate of proton transfer is reasonably fast. We have identified the feasible route of proton transfer from a solvated H^+ to CO_{ads}, which could be written as, $H_5O_2^+{}_{aq} \rightarrow [CO_{ads}\ldots H_5O_2^+{}_{aq}] \rightarrow [CO_{ads}\ldots H_3O^+{}_{aq}] \rightarrow COH_{ads}$.

(iii) In the process of H^+ approaching gradually to the O-end of CO_{ads}, a linear relationship is revealed between the C-O bond distance and the negative charge in CO.

(iv) The formation of CHO_{ads} is a surface catalytic reaction with the coupling between CO_{ads} and H_{ads}. This reaction is endothermic by 0.46 eV with the free energy barrier of 0.64 eV. Before the coupling, H adsorbs first on the surface with a reaction energy of -0.24 eV and the free energy barrier of 0.56 eV.

(v) The formation of COH_{ads} has been found to be more favorable than that of CHO_{ads} kinetically, but CHO_{ads} has been shown to be more stable thermodynamically,

which has further been confirmed by the computational hydrogen electrode model.

This work has revealed that CO activation via the COH intermediate is an important pathway in electrocatalysis, which helps to understand CO_2 electroreduction on Cu electrodes.

Acknowledgements

Financial supports from the NSFC (21361140374, 21321062, 21333003 and 21573183) are acknowledged.

References

[1] Y. Hori, K. Kikuchi, S. Suzuki, Production of CO and CH_4 in electrochemical reduction of CO_2 at metal-electrodes in aqueous hydrogencarbonate solution, Chem. Lett. 14 (1985) 1695-1698.

[2] Y. Hori, K. Kikuchi, A. Murata, S. Suzuki, Production of methane and ethylene in electrochemical reduction of carbon-dioxide at copper electrode in aqueous hydrogencarbonate solution, Chem. Lett. 15 (1986) 897-898.

[3] Y. Hori, A. Murata, R. Takahashi, S. Suzuki, Electroreduction of CO to CH_4 and C_2H_4 at a copper electrode in aqueous-solutions at ambient-temperature and pressure, J. Am. Chem. Soc. 109 (1987) 5022-5023.

[4] M. Gattrell, N. Gupta, A. Co, A review of the aqueous electrochemical reduction of CO_2 to hydrocarbons at copper, J. Electroanal. Chem. 594 (2006) 1-19.

[5] R. J. Lim, M. S. Xie, M. A. Sk, J. M. Lee, A. Fisher, X. Wang, K. H. Lim, A review on the electrochemical reduction of CO_2 in fuel cells, metal electrodes and molecular catalysts, Catal. Today 233 (2014) 169-180.

[6] Y. Hori, H. Wakebe, T. Tsukamoto, O. Koga, Electrocatalytic process of CO selectivity in electrochemical reduction of CO_2 at metal-electrodes in aqueous-media, Electrochim. Acta 39 (1994) 1833-1839.

[7] Y. Hori, I. Takahashi, O. Koga, N. Hoshi, Electrochemical reduction of carbon dioxide at various series of copper single crystal electrodes, J. Mol. Catal. A-Chem. 199 (2003) 39-47.

[8] Y. Hori, I. Takahashi, O. Koga, N. Hoshi, Selective formation of C2 compounds

from electrochemical reduction of CO_2 at a series of copper single crystal electrodes, J. Phys. Chem. B 106 (2002) 15-17.

[9] I. Takahashi, O. Koga, N. Hoshi, Y. Hori, Electrochemical reduction of CO_2 at copper single crystal Cu(S)-[n (111) x (111)] and Cu(S)-[n (110) x (100)] electrodes, J. Electroanal. Chem. 533 (2002) 135-143.

[10] R. L. Cook, R. C. MacDuff, A. F. Sammells, Evidence for formaldehyde, formic-acid, and acetaldehyde as possible intermediates during electrochemical carbon-dioxide reduction at reduction at copper, J. Electrochem. Soc. 36 (1989) 1982-1984.

[11] D. W. DeWulf, T. Jin, A. J. Bard, Electrochemical and surface studies of carbon-dioxide reduction to methane and ethylene at copper electrodes in aqueous-solutions, J. Electrochem. Soc. 136 (1989) 1686-1691.

[12] J. Lee, Y. Tak, Electrocatalytic activity of Cu electrode in electroreduction of CO_2, Electrochim. Acta 46 (2001) 3015-3022.

[13] Y. Hori, A. Murata, R. Takahashi, Formation of hydrocarbons in the electrochemical reduction of carbon-dioxide at a copper electrode in aqueous-solution, J. Chem. Soc., Faraday Trans. 85 (1989) 2309-2326.

[14] J. J. Kim, D. P. Summers, K. W. Frese, Reduction of CO_2 and CO to methane on Cu foil electrodes, J. Electroanal. Chem. 245 (1988) 223-244.

[15] Y. Hori, H. Wakebe, T. Tsukamoto, O. Koga, Adsorption of CO accompanied with simultaneous charge transfer on copper single crystal electrodes related with electrochemical reduction of CO_2 to hydrocarbons, Surf. Sci. 35 (1995) 258-263.

[16] J. K. Norskov, J. Rossmeisl, A. Logadottir, L. Lindqvist, J. R. Kitchin, T. Bligaard, H. Jonsson, Origin of the overpotential for oxygen reduction at a fuel-cell cathode, J. Phys. Chem. B 108 (2004) 17886-17892.

[17] A. A. Peterson, F. Abild-Pedersen, F. Studt, J. Rossmeisl, J. K. Norskov, How copper catalyzes the electroreduction of carbon dioxide into hydrocarbon fuels, Energy Environ. Sci. 3 (2010) 1311-1315.

[18] C. Shi, C. P. O'Grady, A. A. Peterson, H. A. Hansen, J. K. Norskov, Modeling CO_2 reduction on Pt(111), Phys. Chem. Chem. Phys. 15 (2013) 7114-7122.

[19] X. W. Nie, M. R. Esopi, M. J. Janik, A. Asthagiri, Selectivity of CO_2 reduction on copper electrodes: the role of the kinetics of elementary steps, Angew. Chem. Int. Ed. 52 (2013) 2459-2462.

[20] X. W. Nie, W. J. Luo, M. J. Janik, A. Asthagiri, Reaction mechanisms of CO_2 electrochemical reduction on Cu(111) determined with density functional theory, J. Catal. 312 (2014) 108-122.

[21] F. Calle-Vallejo, M. T. M. Koper, Theoretical considerations on the electroreduction of CO to C-2 Species on Cu(100) electrodes, Angew. Chem. Int. Ed. 52 (2013) 7282-7285.

[22] J. S. Filhol, M. Neurock, Elucidation of the electrochemical activation of water over Pd by first principles, Angew. Chem., Int. Ed. 45 (2006) 402-406.

[23] C. D. Taylor, S. A. Wasileski, J. S. Filhol, M. Neurock, First principles reaction modeling of the electrochemical interface: consideration and calculation of a tunable surface potential from atomic and electronic structure, Phys. Rev. B 73 (2006)

165402.

[24] M. Otani, I, Hamada, O. Sugino, Y. Morikawa, Y. Okamoto, T. Ikeshoji, Structure of the water/platinum interface—a first principles simulation under bias potential, Phys. Chem. Chem. Phys. 10 (2008) 3609-3612.

[25] M. Otani, O. Sugino, First-principles calculations of charged surfaces and interfaces: A plane-wave nonrepeated slab approach, Phys. Rev. B 73 (2006) 115407.

[26] Y. H. Fang, G. F. Wei, Z. P. Liu, Theoretical modeling of electrode/electrolyte interface from first-principles periodic continuum solvation method, Catal. Today 202 (2013) 98-104.

[27] S. Schnur, A. Groß, Challenges in the first-principles description of reactions in electrocatalysis, Catal. Today 165 (2011) 129-137.

[28] R. Jinnouchi, A. B. Anderson, Electronic structure calculations of liquid-solid interfaces: Combination of density functional theory and modified Poisson-Boltzmann theory, Phys. Rev. B. 77 (2008) 245417.

[29] A. Y. Lozovoi, A. Alavi, J. Kohanoff, R. M. Lynden-Bell, Ab initio Simulation of Charged Slabs at Constant Chemical Potential. J. Chem. Phys. 115 (2001) 1661-1669.

[30] E. Skulason, V. Tripkovic, M. E. Bjorketun, S. Gudmundsdottir, G. Karlberg, J. Rossmeisl, T. Bligaard; H. Jonsson, J. K. Norskov, Modeling the electrochemical hydrogen oxidation and evolution reactions on the basis of density functional theory calculations J. Phys. Chem. C 114 (2010) 18182-18197.

[31] E. Skulason, G. S. Karlberg, J. Rossmeisl, T. Bligaard, J. Greeley, H. Jonsson, J. K. Norskov, Density functional theory calculations for the hydrogen evolution

reaction in an electrochemical double layer on the Pt(111) electrode, Phys. Chem. Chem. Phys. 9 (2007) 3241-3250.

[32] T. Sheng, W. F. Lin, C. Hardacre, P. Hu, Role of water and adsorbed hydroxyls on ethanol electrochemistry on Pd: new mechanism, active centers, and energetics for direct ethanol fuel cell running in alkaline medium, J. Phys. Chem. C 118 (2014) 5762-5772.

[33] E. Antolini, E. R. Gonzalez, Alkaline direct alcohol fuel cells, J. Power Source 195 (2010) 3431-3450.

[34] K. J. P. Schouten, Z. Qin, E. P. Gallent, M. T. M. Koper, Two pathways for the formation of ethylene in CO reduction on single-crystal copper electrodes, J. Am. Chem. Soc. 134 (2012) 9864-9867.

[35] Y. G. Kim, J. H. Baricuatro, A. Javier, J. M. Gregoire, M. P. Soriaga, The evolution of Polycrystalline Copper Surface, first to Cu(111) and then to Cu(100), at a fixed CO_2RR Potential: A Study by *Operando* EC-STM, Langmuir. 30 (2014) 15053-15056.

[36] G. Kresse, J. Hafner, Ab initio molecular dynamics for open-shell transition metals, Phys. Rev. B 48 (1993) 13115-13118.

[37] G. Kresse, J. Furthmuler, Efficient iterative schemes for ab initio total-energy calculations using a plane-wave basis set. Phys. Rev. B 54 (1996) 11169-11186.

[38] G. Kresse, J. Hafner, Ab initio molecular-dynamics for liquid metals, Phys. Rev. B 47 (1993) 558-561.

[39] G. Kresse, J. Hafnre, Ab initio molecular-dynamics simulation of the

liquid-metal amorphous-semiconductor transition in germanium, Phys. Rev. B 49 (1994) 14251-14269.

[40] G. Kresse, J. Furthmuller, Efficiency of ab-initio total energy calculations for metals and semiconductors using a plane-wave basis set, Comput. Mater. Sci. 6 (1996) 15-50.

[41] P. E. Blochl, Projector augmented-wave method, Phys. Rev. B 50 (1994) 17953-17979.

[42] G. Kresse, D. Joubert, From Ultrasoft pseudopotentials to the projector augmented-wave method, Phys. Rev. B 59 (1999) 1758-1775.

[43] J. P. Pedrew, K. Burke, M. Ernzerhof, Generalized gradient approximation made simple, Phys. Rev. Lett. 77 (1996) 3865-3868.

[44] M. Lingwood, J. R. Hammond, D. A. Hrovat, J. M. Mayer, W. T. Borden, MPW1K performs much better than B3LYP in DFT calculations on reaction that proceed by proton-coupled electron transfer (PCET), J. Chem. Theory Comput. 2 (2006) 740-745.

[45] G. S. Karlberg, J. Rossmeisl, J. K. Norskov, Estimations of electric field effects on the oxygen reduction reaction based on the density functional theory, Phys. Chem. Chem. Phys. 9 (2007) 5158-5161.

[46] M. Sprik, G. Ciccotti, Free energy from constrained molecular dynamics, J. Chem. Phys. 109 (1998) 7737-7744.

[47] P. Carloni, M. Sprik, W. Andreoni, Key steps of the *cis*-Platin-DNA interaction: density functional theory-based molecular dynamics simulations, J. Phys. Chem. B

104 (2000) 823-835.

[48] T. Bucko, Ab initio calculations of free-energy reaction barriers, J. Phys.: Condens. Matter 20 (2008) 064211.

[49] J. Lecoeur, J. P. Bellier, Potentiels de charge nulle d'electrodes monocristallines de cuivre d'orientation (111) et (100) au contact de solutions aqueuses de perchlorate de potassium, Electrochim. Acta 30 (1985) 1027-1033.

[50] P. S. Bagus, C. J. Nelin, W. Muller, M. R. Philpott, H. Seki, Field-induced vibrational frequency shifts of CO and CN Chemisorbed on Cu(100), Phys. Rev. Lett. 58 (1987) 559-562.

[51] M. J. Weaver, Electrostatic-field effects on adsorbate bonding and structure at metal surfaces-parallels between electrochemical and vacuum systems, Appl. Surf. Sci., 67 (1993) 147-159.

[52] X. Sun, X. Cao, P. Hu, Theoretical insight into the selectivities of copper-catalyzing heterogeneous reduction of carbon dioxide, Sci. China Chem. 58 (2015) 553-564.

[53] G. F. Wei, Y. H Fang, Z. P. Liu, First principles tafel kinetics for resolving key parameters in optimizing oxygen electrocatalytic reduction catalyst, J. Phys. Chem. C 116 (2012) 12696-12705.

Figure Captions

Figure 1. Model of the charged water/Cu(100) interface including 20 water molecules, a solvated proton (H^+) in $H_5O_2^+$, adsorbed CO (CO_{ads}) and negatively charged Cu(100) slab. Orange: Cu; grey: C; red: O; white: H.

Figure 2. Electrostatic potential profile averaged on the surface plane as a function of the z-axis. The blue line was calculated from the neutral system and the red line from the charged system with H^+ highlighted by yellow. In the vacuum region, a dipole correction is introduced in the calculation in order to electrostatically decouple the periodically repeated slabs in the z-direction.

Figure 3. Free energy profile for the formation of COH_{ads}, $CO_{ads} + H^+ + e^- \rightarrow COH_{ads}$.

Figure 4. Structures in the formation of COH_{ads} ($CO_{ads} + H^+ + e^- \rightarrow COH_{ads}$) obtained from *ab initio* MD simulations.

Figure 5. Calculated negative charges (a) and C-O bond distances (b) in CO fragment when H^+ approaches the O-end of CO_{ads} from 1.8 Å to 1.0 Å.

Figure 6. Linear relationship between the C-O bond distance and negative charge in CO fragment under different conditions. CO_v: CO adsorption at Cu(100) without water; CO_{aq}: CO adsorption at the water/Cu(100) interface; CO_{aq}^*: CO adsorption at the charged water/Cu(100) interface; COH_v: COH adsorption at Cu(100) without water; COH_{aq}: COH adsorption at the water/Cu(100) interface; and CO: CO molecule in vacuum as a reference.

Figure 7. Free energy profiles for the formation of CHO_{ads}. (a) $H^+ + e^- \rightarrow H_{ads}$; (b)

$CO_{ads} + H_{ads} \rightarrow CHO_{ads}$.

Figure 8. Structures in the formation of CHO_{ads} ($H^+ + e^- \rightarrow H_{ads}$, $CO_{ads} + H_{ads} \rightarrow CHO_{ads}$) obtained from *ab initio* MD simulations.

Figure 9. Comparison of two pathways for the formations of COH_{ads} (red) and CHO_{ads} (blue) in CO activation on Cu(100).

Figure 10. Comparison of two free energy profiles for the formations of COH_{ads} (red) and CHO_{ads} (blue) in CO activation on Cu(100) using computational hydrogen electrode model. The solid line represents 0 V (vs SHE) condition and the dashed line -2.04 V (vs SHE).

Figure 11. (a) Free energies as a function of H_{ads} coverage from 0 ML to 0.89 ML for the formations of COH_{ads} and CHO_{ads}. (b) Free energy changes of $H_{ads} \rightarrow 1/2\ H_2$ as a function of H_{ads} coverage from 0.11 ML to 1 ML.

Figure 1

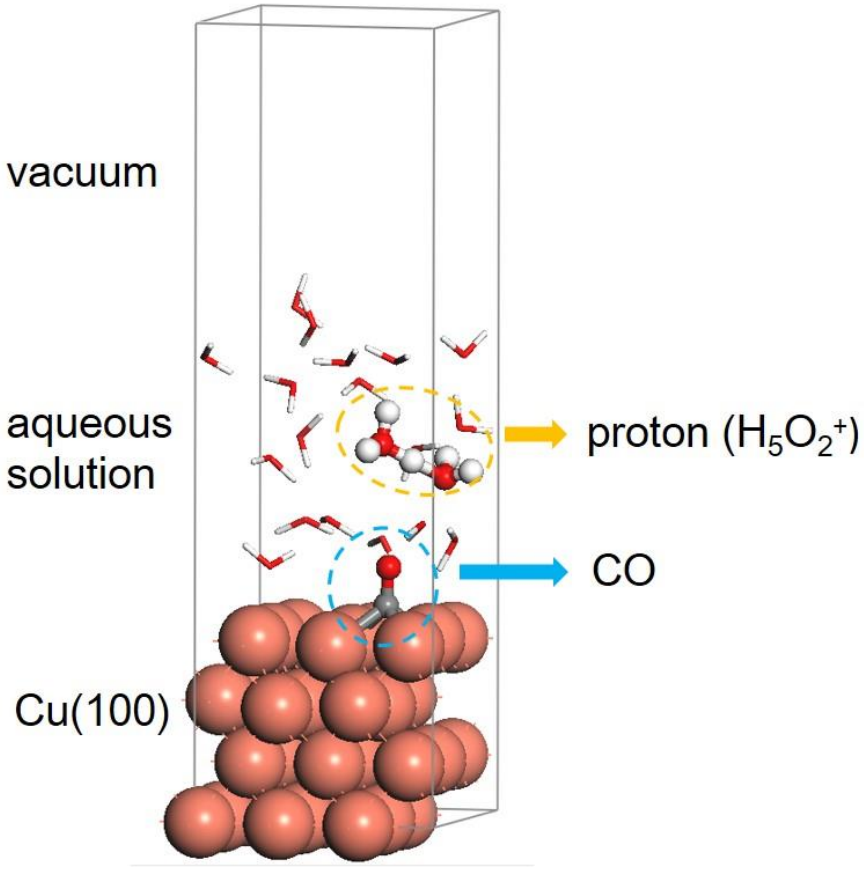

Figure 2

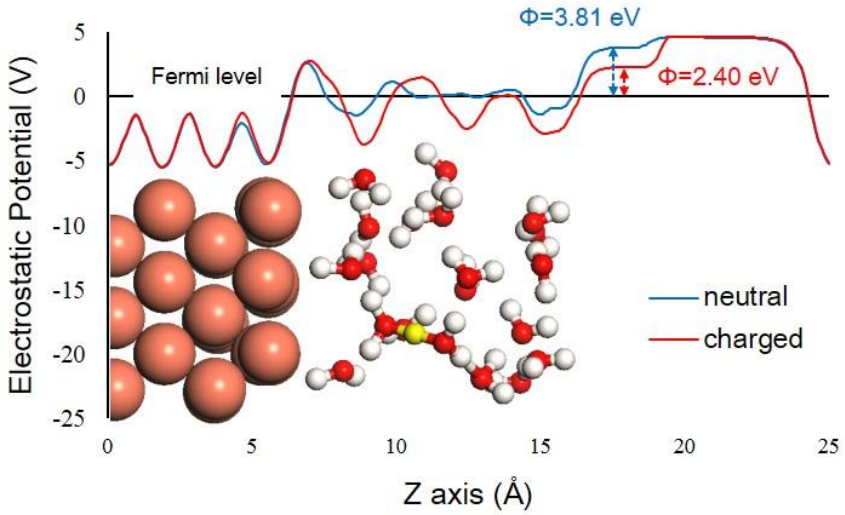

Figure 3

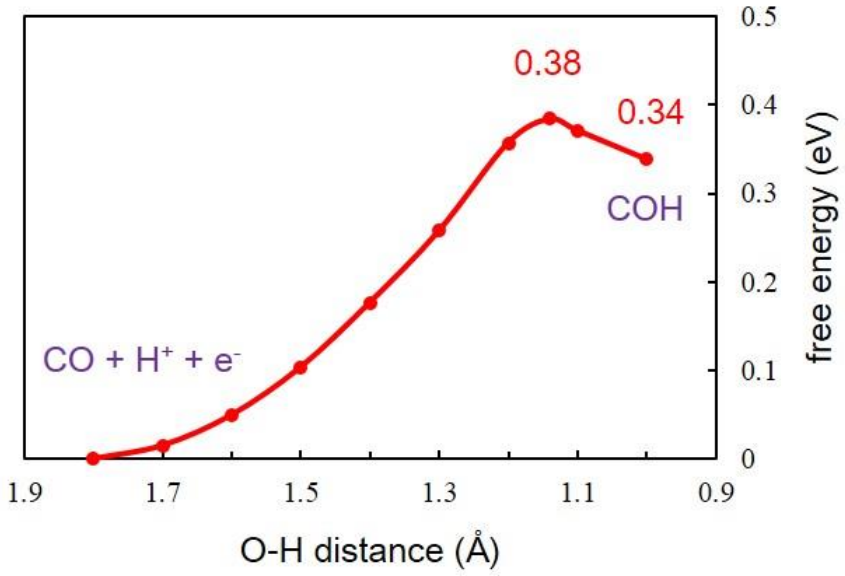

Figure 4

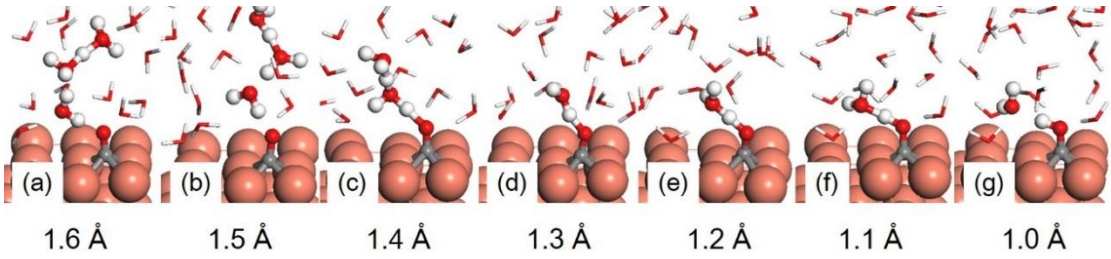

Figure 5

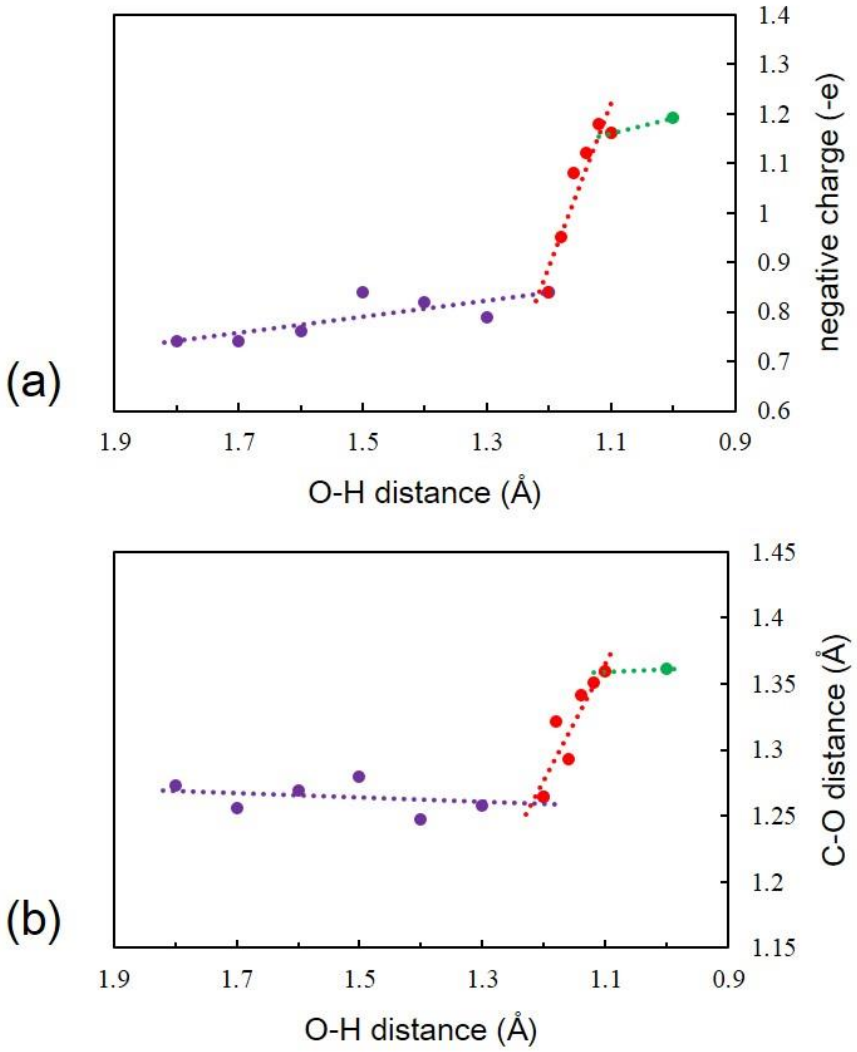

Figure 6

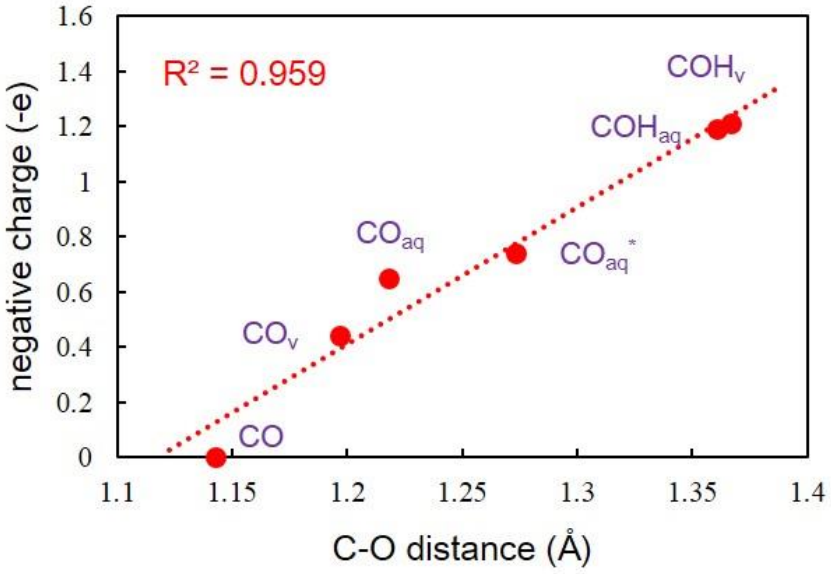

Figure 7

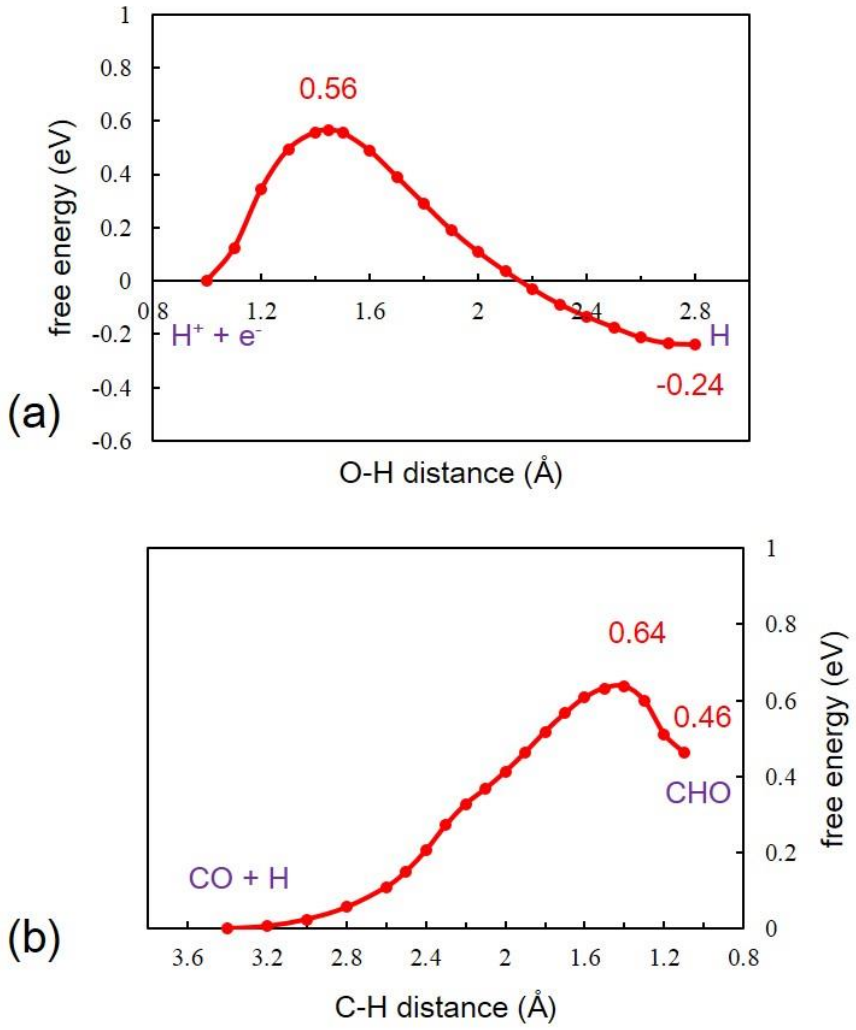

Figure 8

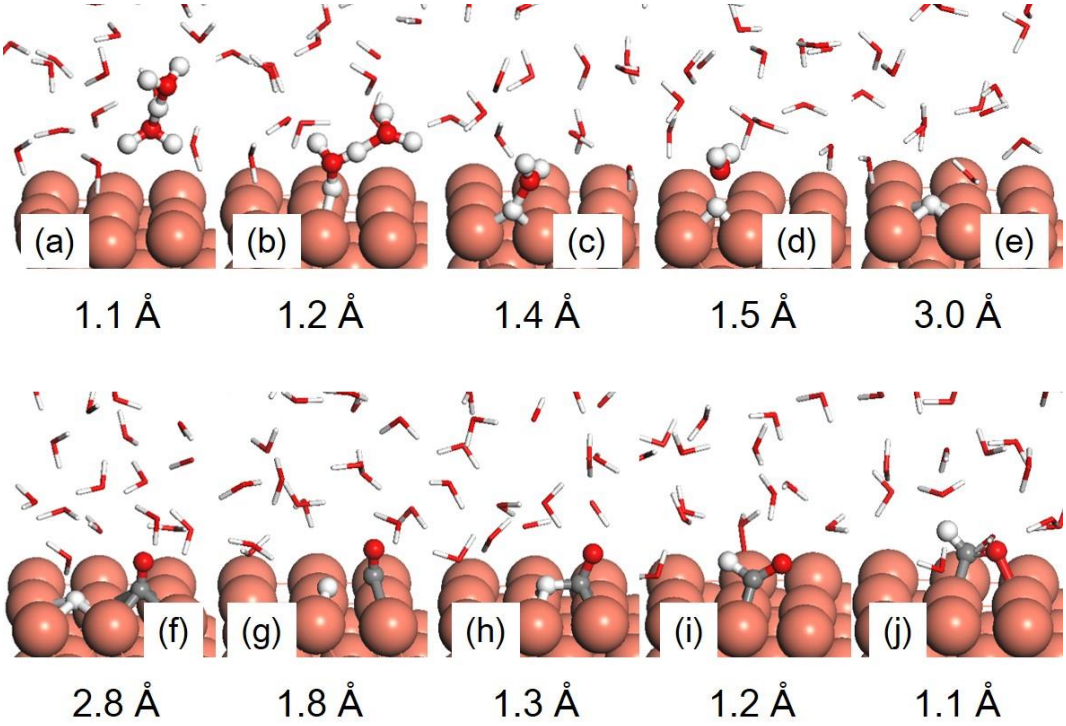

Figure 9

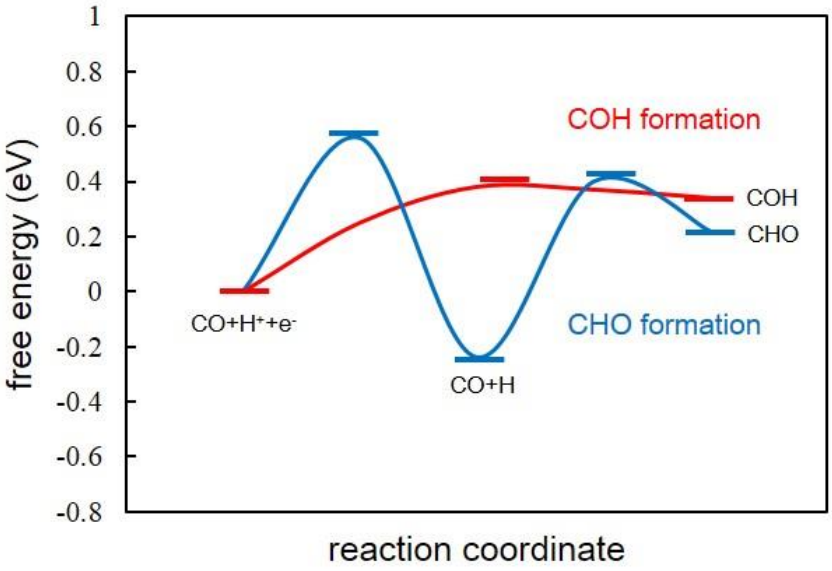

Figure 10

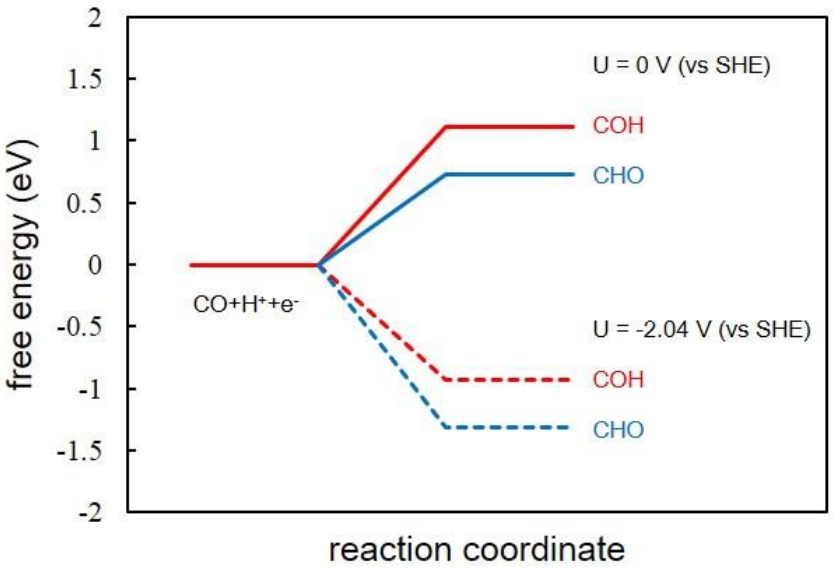

Figure 11

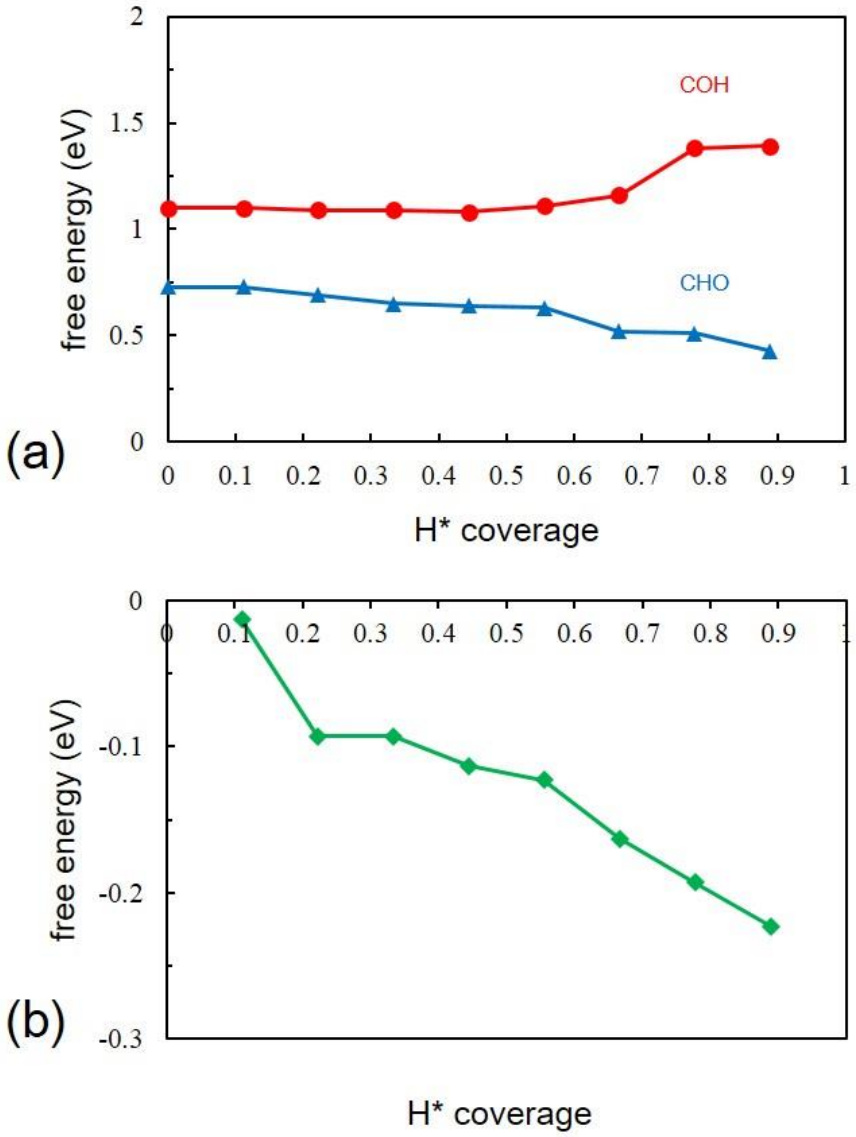

Tables

Table 1. Negative charges (e) in CO_{ads}, first Cu layer and Cu bulk under three conditions: at Cu(100) without water, at the water/Cu(100) interface and the charged water/Cu(100) interface.

	CO_{ads}	first Cu layer	Cu bulk
Cu(100)	-0.44	0.32	0.12
water/Cu(100)	-0.65	0.43	0.24
charged water/Cu(100)	-0.74	0.26	-0.05

Table 2. Calculated C-O bond distance (Å) and negative charges (e) and in CO fragment with the distance between H^+ and O-end of CO_{ads}.

d(O-H)	d(C-O)	charge
1.8	1.273	-0.74
1.7	1.256	-0.74
1.6	1.269	-0.76
1.5	1.280	-0.84
1.4	1.247	-0.82
1.3	1.258	-0.79
1.2	1.264	-0.84
1.18	1.321	-0.95
1.16	1.293	-1.08
1.14	1.341	-1.12
1.12	1.351	-1.18
1.1	1.359	-1.16
1.0	1.361	-1.19

Table 3. Calculated C-O bond distance (Å) and negative charges (e) in CO fragment under different conditions. CO_v: CO adsorption at Cu(100) without water; CO_{aq}: CO adsorption at the water/Cu(100) interface; CO_{aq}^*: CO adsorption at the charged water/Cu(100) interface; COH_v: COH adsorption at Cu(100) without water; COH_{aq}: COH adsorption at the water/Cu(100) interface; and CO: CO molecule in vacuum as a reference.

	d(C-O)	charge
CO molecule	1.143	0
CO_v	1.197	-0.44
CO_{aq}	1.218	-0.65
CO_{aq}^*	1.273	-0.74
COH_v	1.367	-1.21
COH_{aq}	1.361	-1.19

Table 4. Calculated the C-O bond distances (Å) and negative charges (e) in CO_{ads} under different electric fields (V/Å).

electric field	d(C-O)	d(C-O)[ref[50]]	charge
-0.52	1.191(-0.006)	1.117(-0.005)	-0.440
0	1.197	1.122	-0.442
0.52	1.203(0.006)	1.127(0.005)	-0.443